JOURNAL OF Applied Polymer SCIENCE

Special Issue: Manufacturing of Advanced Biodegradable Polymeric Components

Guest Editors: Prof. Roberto Pantani (University of Salerno) and
Prof. Lih-Sheng Turng (University of Wisconsin–Madison)

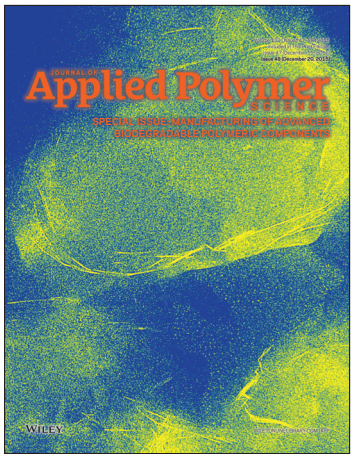

EDITORIAL

REVIEWS

ARTICLES

JOURNAL OF Applied Polymer SCIENCE

Special Issue: Manufacturing of Advanced Biodegradable Polymeric Components

Guest Editors: Prof. Roberto Pantani (University of Salerno) and Prof. Lih-Sheng Turng (University of Wisconsin–Madison)

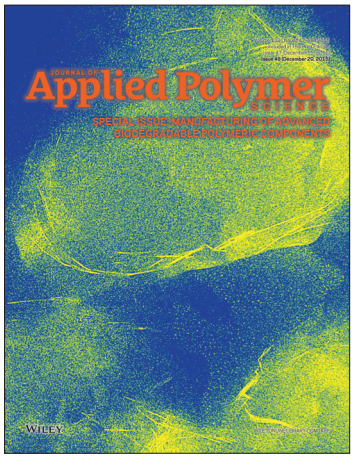

Rotational molding of biodegradable composites obtained with PLA reinforced by the wooden backbone of opuntia ficus indica cladodes
A. Greco and A. Maffezzoli, *J. Appl. Polym. Sci.* 2015, **DOI:** 10.1002/app.42447

Foam injection molding of poly(lactic) acid: Effect of back pressure on morphology and mechanical properties
V. Volpe and R. Pantani, *J. Appl. Polym. Sci.* 2015, **DOI:** 10.1002/app.42612

Modification and extrusion coating of polylactic acid films
H.-Y. Cheng, Y.-J. Yang, S.-C. Li, J.-Y. Hong and G.-W. Jang, *J. Appl. Polym. Sci.* 2015, **DOI:** 10.1002/app.42472

Processing and properties of biodegradable compounds based on aliphatic polyesters
M. R. Nobile, P. Cerruti, M. Malinconico and R. Pantani, *J. Appl. Polym. Sci.* 2015, **DOI:** 10.1002/app.42481

Journal of Applied Polymer Science

Oriented polyvinyl alcohol films using short cellulose nanofibrils as a reinforcement

Jun Peng,[1,2] Thomas Ellingham,[1,2] Ronald Sabo,[3] Craig M. Clemons,[3] Lih-Sheng Turng[1,2]

[1]Polymer Engineering Center, University of Wisconsin-Madison, Madison, Wisconsin 53706

[2]Wisconsin Institute for Discovery, University of Wisconsin-Madison, Madison, Wisconsin 53715

[3]USDA Forest Service, Forest Products Laboratory, Madison, WI 53726

Correspondence to: L.-S. Turng (E-mail: turng@engr.wisc.edu)

ABSTRACT: Short cellulose nanofibrils (SCNF) were investigated as a new kind of reinforcement for polyvinyl alcohol (PVA) films. SCNF were mechanically isolated from hardwood pulp after enzymatic pretreatment. Various concentrations of SCNF were added to an aqueous PVA solution, which were cast into composite films and then hot drawn with various draw ratios at 200°C. SCNF were effective in improving PVA film tensile properties (i.e., ultimate strength and elastic modulus), which depended on SCNF loading, PVA crystal orientation, and the draw ratio. For example, the ultimate strength and modulus of a composite film with a SCNF weight ratio of 3% and a draw ratio of 7.5 were nearly 46 and 61% higher than that of the neat PVA. The PVA crystal orientation increased when small amounts of SCNF were added but decreased as the SCNF content increased above about 6%, likely due to SCNF percolation resulting in network formation that inhibited alignment. Stress-induced crystallization during hot drawing increased the crystallinity of PVA in both the PVA and its composites. Cryogenic and tensile-fractured SEM images of PVA/SCNF composite films showed a uniform SCNF dispersion in the PVA matrix. Young's moduli of drawn composite films were predicted surprisingly well by the rule of mixtures except at intermediate levels of SCNF where the increased orientation of the matrix was not considered in the model. © 2015 Wiley Periodicals, Inc. J. Appl. Polym. Sci. **2015**, *132*, 42283.

KEYWORDS: cellulose and other wood products; composites; mechanical properties; nanoparticles; nanowires and nanocrystals; X-ray

Received 20 November 2014; accepted 31 March 2015

DOI: 10.1002/app.42283

INTRODUCTION

Renewable and biodegradable cellulose is the most abundant natural biopolymer in the world. Fibrils, which are discrete, micro- or nanoscale fibers extracted from cellulose, have superior mechanical properties and extraordinary potential to improve the mechanical performance of polymeric matrices. Trees, plants, some marine creatures such as tunicates, and certain bacteria and algae form microfibrils, fine threadlike structures made from stacks of cellulose molecules. These microfibrils have a complex structural hierarchy and often act as the main reinforcing element in their respective organisms.[1] In part, it is the high reinforcing potential of the native crystalline cellulose within these microfibrils that has recently led researchers to extract nanocellulose from microfibrils for use in composites. Several mechanical approaches, such as refining,[2] homogenizing,[3] cryocrushing,[4] and high intensity ultrasonic treatment, have been employed to isolate cellulose fibrils from wood or plant fibers.[5] Cellulose nanofibrils (CNF) (also called nanofibrillated cellulose) are obtained by mechanical isolation, often after chemical or enzymatic pretreatment. CNF contains both amorphous and crystalline regions and typically have high aspect ratios (4–20 nm in width, 500–2000 nm in length[1]). Cellulose nanocrystals (CNC) are produced by acid hydrolysis, during which most of the amorphous fraction is removed. Depending on preparation and measurement methods, tensile moduli of 20–100 GPa have been reported for CNF.[6] The moduli of CNC are expected to be higher due to their highly crystalline nature, but somewhat lower than the Young's modulus of 138 GPa reported for native cellulose I crystals.[7] As a result, nanocellulose (CNF or CNC) has emerged as a new class of naturally sourced reinforcements for polymer composites. However, some challenges still exist to efficiently use nanocellulose as reinforcing fillers. For example, preparation of nanocellulose results in aqueous gels or suspensions that are not easily incorporated into most polymers. Also, nanocellulose is very hydrophilic, which can create difficulties in dispersing in and bonding with many polymers. To overcome these obstacles, water-soluble polymers are often considered as suitable candidates for conceivably easy dispersion of nanocellulose.

Table I. Compositions of Aqueous PVA/SCNF Solutions and Dried Films

	Weights used in preparing solutions (g)			Concentrations in solution (wt %)		
Sample	20 wt % PVA solution	1 wt % SCNF suspension	Added water	PVA	SCNF	SCNF/PVA ratio in dry film (%)
Pure PVA	60	0	73.3	9	0	0
PVA/SCNF1	60	12	61.3	9	0.09	1
PVA/SCNF2	60	24	49.3	9	0.18	2
PVA/SCNF3	60	36	37.3	9	0.27	3
PVA/SCNF6	60	72	1.3	9	0.54	6
PVA/SCNF9	60	108	0	7	0.64	9
PVA/SCNF12	60	144	0	6	0.71	12

Polyvinyl alcohol (PVA) is a biodegradable and biocompatible synthetic polymer with a broad range of industrial and technical applications (e.g., coatings, adhesives, and water-soluble packaging). The global production of PVA is steadily increasing, with production in 2013 reaching about 2.3 million tons.[8,9] Because of its wide use, water solubility, and ability to hydrogen bond, it has also been of interest as a matrix polymer in nanocellulose composites. PVA–nanocellulose composites have been investigated for a variety of uses including water-responsive mechanically adaptive substrates for medical devices,[10] oil absorbing aerogels,[11] and barrier membranes.[12] While PVA films still only have minor relevance commercially, their performance may be enhanced by applying new technologies, thus leading to new opportunities. Here we investigate the reinforcement of PVA film by a new type of nanocellulose.

Most research on PVA/nanocellulose composites has involved cast films, in which there is little or no alignment of the nanocellulose or PVA.[13–19] However, there has been recent interest in using nanocellulose in oriented PVA composites, although these efforts do little to distinguish the effect of reinforcement and alignment on the mechanical properties of the composites. For example, nanocellulose has been investigated as a reinforcement in PVA fibers[20–23] that could potentially be used to reduce bulk weight and improve strength of cement, for example.[24,25] Uddin *et al.*[20] produced gel spun fibers from aqueous PVA solutions with up to 30% CNC prepared by acid hydrolysis and found 5% CNC could achieve the max tensile properties. However, since adding 5% CNC also led to the highest levels of orientation at a maximum draw, it is not clear whether the improvement resulted from improved orientation or from reinforcement by the CNC. Peresin *et al.*[26] produced PVA mats with up to 15% CNC by electrospinning and found that CNC increased the storage modulus. Endo *et al.*[22] investigated gel-spun PVA fibers reinforced with CNF prepared using 2,2,6,6-tetramethylpiperidine-1-oxy radical (TEMPO)-mediated oxidation as a pretreatment prior to mechanical disintegration. Adding only 1 wt % CNF did not increase tensile strength but further addition of CNF was not possible because of high solution viscosity and gelling of the high aspect ratio fibrils. Thus, shorter fibrils may allow concentrations greater than 1% to be used.

In this study, we investigated a new type of short cellulose nanofibrils (SCNF) that was mechanically isolated from enzymatically pretreated wood pulp as a reinforcement for PVA films. Hopefully, this SCNF could be more easily used to produce oriented composites at higher weight percentages, compared to CNF reported previously, but without the need for concentrated sulfuric acid hydrolysis as in CNC production. Also, since SCNF have more hydroxyl groups available, thus increasing the possibility of greater hydrogen bonding with PVA than CNC, improved mechanical performance may be possible. PVA/SCNF composites were prepared from films cast from homogeneous solutions and subsequently drawn. This approach allowed a wide range of draw ratios to be achieved more easily than with fiber preparation methods. Furthermore, the contributions of orientation and reinforcement on the mechanical properties of the composites were explored and are discussed here. Effects of drawing and SCNF content on the tensile properties of PVA/SCNF composite films, the matrix crystal orientation, and the thermal properties were also investigated.

EXPERIMENTAL

Preparation of Short Cellulose Nanofibrils (SCNF)

SCNF were prepared at the U.S. Forest Service, Forest Products Laboratory (Madison, WI), according to the procedure described by.[27,28] Briefly, a commercial hardwood bleached eucalyptus Kraft pulp (Aracruz Cellulose, Brazil) was soaked in distilled water for 24 h before mechanically disintegrating it in a blender for 10 min. The Kraft pulp was previously analyzed at the Forest Products Laboratory, Madison, WI, to have 92.9% glucan, 5.7% xylan, and 1.2% Klason lignin content. The fiber slurry was then concentrated to 1.5 wt % pulp fiber by centrifuging. Commercial endoglucanase (FiberCare, Novozymes, Franklin, NC) was mixed with pulp fibers at 10% solids and incubated in a flask on a shaker table at 50°C for 24 h at 200 rpm. The enzymatically treated pulp fiber was then rinsed with distilled water and then fibrillated using a Super Mass Colloider (MKZA6-2, Masuko Sangyo, Japan). During fibrillation, the wet pulp fiber was ground between two-stone disks with a gap of 100 μm and a rotation speed of 1,500 rpm. Approximately 100 g of pulp fiber (dry basis) were refined in circulation for 6 h. The suspension was further processed by running it 15 times through a microfluidizer (M-110EH-30, Microfluidics, MA) with 200 and 87 μm chambers in sequence under a

pressure of 150 MPa. The resulting SCNF suspension was stored in a cold room (4°C) until used.

Preparation of PVA/SCNF Cast Films

A 99% hydrolyzed commercial-grade of PVA from Sigma-Aldrich with a weight-average molecular weight of 85,000 to 124,000 was used as the matrix polymer. A sufficient amount of PVA was dissolved in water at 90°C with mechanical stirring for 30 min to yield 20% PVA by weight. Solutions for casting films were prepared by mixing various amounts of SCNF solution, PVA solution, and water at 90°C for 60 min. Specific compositions are listed in Table I. The PVA/SCNF solutions were volumetrically poured into petri dishes and dried at room temperature, followed by vacuum drying at 95°C for 4 h. The vacuum drying temperature and duration were chosen to facilitate drying but minimize material degradation and yellowing.

Film Hot Drawing

The dried PVA/SCNF films were cut into 50.8 mm (length) by 6.35 mm (width) strips for hot drawing and characterization. The strips were first clamped to a customized stretching rig and then preheated for 1.5 min at 200°C, which is well below the neat PVA melting temperature of 230°C. The films were then drawn at a rate of 152.4 cm (6 in.) per min at 200°C. The total drawing cycle was completed in 3–4 min. The sample strips maintained a similar transparency and color suggesting no obvious thermal degradation. The draw ratio was defined as the final length of the sample divided by the original length. Draw ratios of 1, 7.5, and the maximum draw ratio were investigated.

Transmission Electron Microscopy (TEM)

The SCNF structure and dimensions were investigated by TEM. A few drops of diluted SCNF solution (0.5 wt % in water) were deposited on a TEM copper grid and dried. The sample grids were analyzed using a Philips CM-100 TEM (Philips/FEI Corporation, Holland) at an accelerating voltage of 100 kV. ImageJ software (1.48d, developed by National Institutes of Health) was used to measure the length and diameter range based on the TEM images.

Scanning Electron Microscopy (SEM)

The outside surfaces and cryogenic and tensile fracture surfaces of undrawn and hot-drawn PVA/SCNF strips were analyzed by a scanning electron microscope (SEM; Model LEO 1530, JEOL, Japan) at an accelerating voltage of 3 kV.

Wide-Angle X-ray Diffraction (WAXD)

X-ray diffraction patterns were obtained with a Bruker diffractometer (D8 Discovery, Bruker) by irradiating the PVA/SCNF film with Cu Kα radiation perpendicular to the film stretching direction. The accelerating voltage and current were 50 kV and 1 mA, respectively. PVA crystal orientation was determined using the most intense equatorial diffraction spots, those corresponding to the $(101/10\bar{1})$ planes. The crystal orientation was described by Herman's orientation parameter (f), as defined by eqs. (1) and (2),[29]

$$f = \frac{3\cos^2\varphi - 1}{2} \quad (1)$$

$$\cos^2\varphi = \frac{\sum_0^{\pi/2} I(\varphi)\sin\varphi\cos^2\varphi}{\sum_0^{\pi/2} I(\varphi)\sin\varphi} \quad (2)$$

where φ is the azimuthal angle and $I(\varphi)$ is the intensity along the Debye–Scherrer ring. It was not possible to determine the orientation of the SCNF due to the small amount added and peak overlap. However, it is likely that the SCNF is also oriented somewhat during drawing.

Tensile Testing

Tensile properties were measured using a tensile testing machine (Instron, MA) with a 30 N load cell, a gauge length of 25.4 mm, and an extension rate of 0.254 cm/min following the ASTM D3379-75 standard.[30] All specimens were dried in a vacuum oven at 95°C for 4 h prior to testing. The experimental results were evaluated as an average of 10 measurements.

Thermal Properties

Differential scanning calorimetry (DSC, Model Q2000, TA Instrument, New Castle, DE) was employed to investigate the melting temperature (T_m), enthalpy of fusion (ΔH_f), crystallinity (χ_c), and crystallization temperature of the PVA. DSC analyses were performed between −20 and 250°C, with heating and cooling rates of 10°C/min. A heat of fusion of 150 J/g for 100% crystalline PVA was used in determining PVA crystallinity in our samples.[31] Thermogravimetric analysis (TGA model Q50, TA Instrument, New Castle, DE) was used to analyze the decomposition temperature of neat and filled PVA films. All TGA tests were performed between 25 and 800°C, with a heating rate of 10°C/min. All specimens were dried in a vacuum oven at 95°C for 4 h prior to testing.

RESULTS AND DISCUSSION

Oriented PVA/SCNF Films

Figure 1 shows a TEM image of the morphology of the SCNF prepared by enzymatic pretreatment and mechanical refining. Image analysis yielded estimates of the length and diameter of 294 ± 95 and 13.6 ± 3.2 nm, respectively. The aspect ratios of about 15–28 were similar to that found for cellulose nanocrystals (CNC) produced by sulfuric acid hydrolysis.[1] Based on the XRD pattern of the 100% cast SCNF film, the crystallinity of the SCNF was determined to be 80%,[22] which is comparable to that of CNC.[1,26] However, the SCNF have more available hydroxyl groups than the sulfuric acid hydrolyzed CNC, in which many of the hydroxyl groups are sulfated during its preparation. This may result in an improved ability of the SCNF to form hydrogen bonds with the PVA matrix. Furthermore, because of the short aspect ratios of SCNF, they can be much easier to disperse in PVA solutions at high filler concentrations as compared to enzymatically pretreated cellulose nanofibrils that have not been microfluidized and have higher aspect ratios. This has been problematic in past research.[22] For example, higher aspect ratio CNF were unable to disperse uniformly in the PVA gel spinning dope and formed gels if the CNF weight ratio was above 1%.[22,32] Generally speaking, relatively high filler weight ratios and good dispersion are critical for improving the mechanical performance of polymeric matrices.

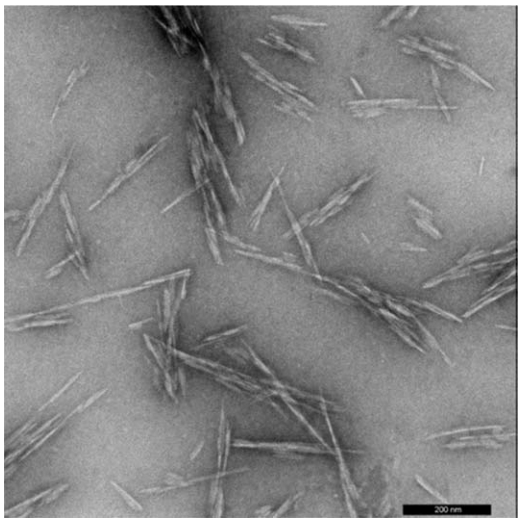

Figure 1. TEM image of SCNF; the scale bar is 200 nm.

In this study, PVA/SCNF solutions with SCNF weight ratios of 1–12% were cast and then dried into thin films. The PVA/SCNF strips cut from the cast films were hot drawn at 200°C to improve PVA and SCNF orientation. The tensile properties and micromorphologies of stretched neat PVA samples greatly depend on chain extension and molecular orientation, which are largely controlled by drawing.[33,34] Since high temperatures can increase the mobility of molecular chains as well as the reinforcing fillers in the polymeric matrix, hot drawing is a preferred process for improving the mechanical performance of PVA/SCNF composite films.

The consistently achievable maximum hot draw ratio (DR) for neat PVA was 11.3, which decreased slightly as SCNF were added (Table II). Apparently, the presence of SCNF filler inhibited drawing of the filled PVA films due to the strong interfacial bonding between the SCNF and the PVA matrix. As a comparison, 5 wt % CNC was reported to improve the drawability of PVA fiber[33] The reduced maximum draw ratio in this work was attributed to stronger hydrogen bonds between the PVA and the SCNF, as compared to that between the PVA and the CNC. To investigate the effects of hot-drawing on PVA crystal orientation and composite tensile properties, the PVA/SCNF samples with another draw ratio were also chosen: draw ratio of 7.5—two-thirds of the maximum hot draw ratio.

Crystal Orientation Analysis

Wide angle X-ray diffraction (WAXD) was used to probe PVA crystal orientation, which depends on amount of drawing (Figure 2). The geometry of the X-ray experiment is shown in the insert in Figure 2(a). The brightest broad arc in Figure 2(a) of PVA/SCNF12 with no drawing indicates partial PVA $(101/10\bar{1})$ crystal orientation. This partial orientation is likely formed due to stresses developed during drying of the cast film. The equatorial bright spots in Figure 2(b), which are attributed to the $(101/10\bar{1})$ and (200) planes, implied strong PVA crystal alignment in the hot drawn films along the stretching direction. Some orientation of SCNF is also likely in the drawn films. However, since little SCNF was added, and the characteristic $(101/10\bar{1})$ plane diffraction patterns of PVA overlapped those of SCNF's, there were no discernible or isolated patterns that could be attributed to SCNF. Thus, the X-ray diffraction patterns of PVA/SCNF films were only employed to quantify the crystal orientation of PVA.

Crystal orientation was calculated based on Herman's orientation parameter (f) according to eqs. (1) and (2). Table II summarizes the crystal orientation from the diffraction peaks for the $(101/10\bar{1})$ planes of pure PVA and composites films with various draw ratios (i.e., 1, 7.5, and the maximum draw ratio). When the draw ratio was 1, we performed no hot drawing and the sample films had a Herman's orientation parameter of ~0.58, indicating lower crystal orientation than in the highly drawn films. The slight orientation of the unstretched film was most likely due to the surface tension developed during drying. The PVA crystal orientation increased as the draw ratio rose.

In addition to their impact on draw ratios, SCNF concentration also influenced PVA crystal orientation during drawing. Small amounts of SCNF fillers with weight ratios of 6% or less appeared to facilitate orientation, increasing the Herman's orientation parameter (f). At higher SCNF contents, however, orientation was reduced likely because SCNF network formation hindered molecular alignment, which may have resulted as the SCNF exceeded the percolation threshold. For rod-like nanoparticles, the percolation threshold (Φ_c) can be related to the aspect ratio of the nanoparticles by the following equation:[35]

Table II. Herman's Orientation Parameter (f) of Pure PVA and PVA/SCNF Films with Various Draw Ratios (DR) Based on the Diffraction Peaks for the (101/10) Planes

Sample	DR1	DR7.5	DR_{max}	Max hot draw ratio at 200°C
Pure PVA	0.58	0.80	0.90	11.3
PVA/SCNF1	0.58	0.83	0.91	11.0
PVA/SCNF2	0.59	0.85	0.92	11.0
PVA/SCNF3	0.59	0.86	0.94	10.9
PVA/SCNF6	0.59	0.85	0.91	10.9
PVA/SCNF9	0.58	0.81	0.91	10.7
PVA/SCNF12	0.57	0.81	0.91	10.5

DR1 corresponds to undrawn samples.

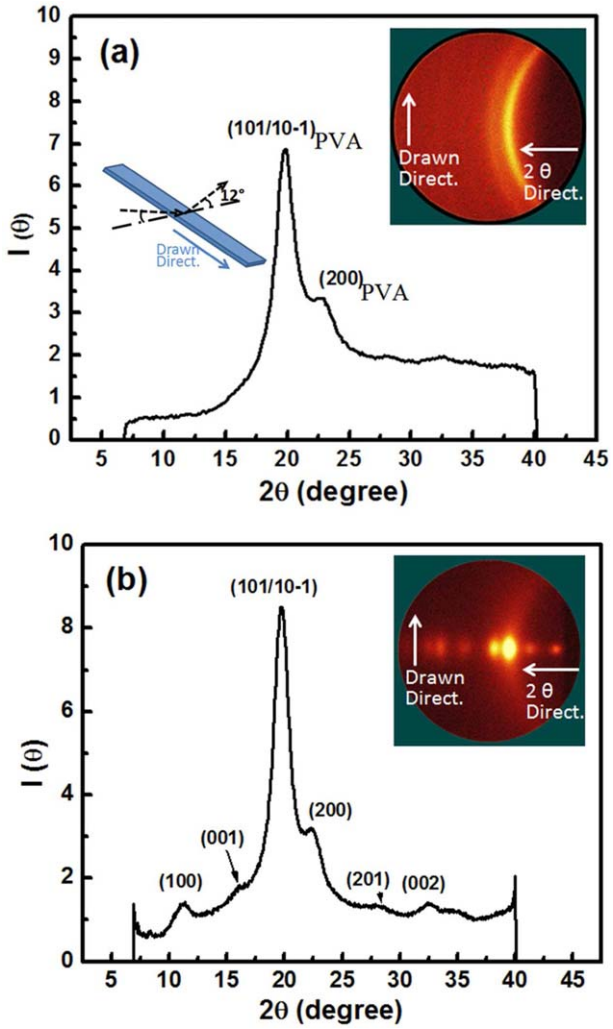

Figure 2. X-ray diffraction intensity as a function of 2θ: (a) PVA/SCNF12 with a draw ratio of 1.0 (i.e., unstretched), and (b) PVA/SCNF12 with a draw ratio of 7.5. Inset in upper right corners are the WAXD patterns. The inset in Figure 2(a) shows the geometry of the tests. [Color figure can be viewed in the online issue, which is available at wileyonlinelibrary.com.]

$$\Phi_c = \frac{0.7}{L/d} \tag{3}$$

In eq. (3), L/d is the aspect ratio of the fiber filler, which assumes a cylindrical shape. The calculated percolation threshold based on the SCNF aspect ratio determined by TEM was about 2.5–4.7%. Therefore, when the SCNF weight ratio exceeds about 3%, a network can form, which could hinder PVA chain mobility and, consequently, crystal orientation. As a result, adding small amounts of SCNF filler will facilitate orientation, but too high of a filler weight ratio became an obstacle to orientation.

Tensile Properties

Tensile tests were performed to quantify SCNF reinforcement of PVA films. Representative stress–strain curves of composite films with various SCNF weight ratios are shown in Figure 3. The ultimate strength and Young's modulus of films with draw ratios of 1.0 and 7.5 are listed in Table III. Adding SCNF to PVA films generally yielded stronger, stiffer, and sometimes tougher films. As shown in Figure 3(a), the tensile moduli of undrawn composite PVA films increased proportionally with the addition of SCNF. The ultimate strength of PVA/SCNF films rose with SCNF content and then remained relatively constant above an SCNF weight ratio of 6%. However, the strain-at-break was negatively affected by the addition of SCNF. A similar trend in tensile properties of filled PVA film with a higher draw ratio of 7.5 is indicated in Figure 3(b). The values of the ultimate strength and Young's moduli were much higher compared with their counterparts of the same composition but with a draw ratio of 1.0 due to the polymer orientation (and possibly SCNF orientation) as is evidenced by the measured PVA crystal orientation. However, tensile properties of composite films at maximum draw ratios were highly variable and are not presented. This large variability is likely due to being overdrawn, resulting in damage development during drawing.

PVA crystal orientation in hot drawn films also crucially affects the mechanical properties in addition to the reinforcement from

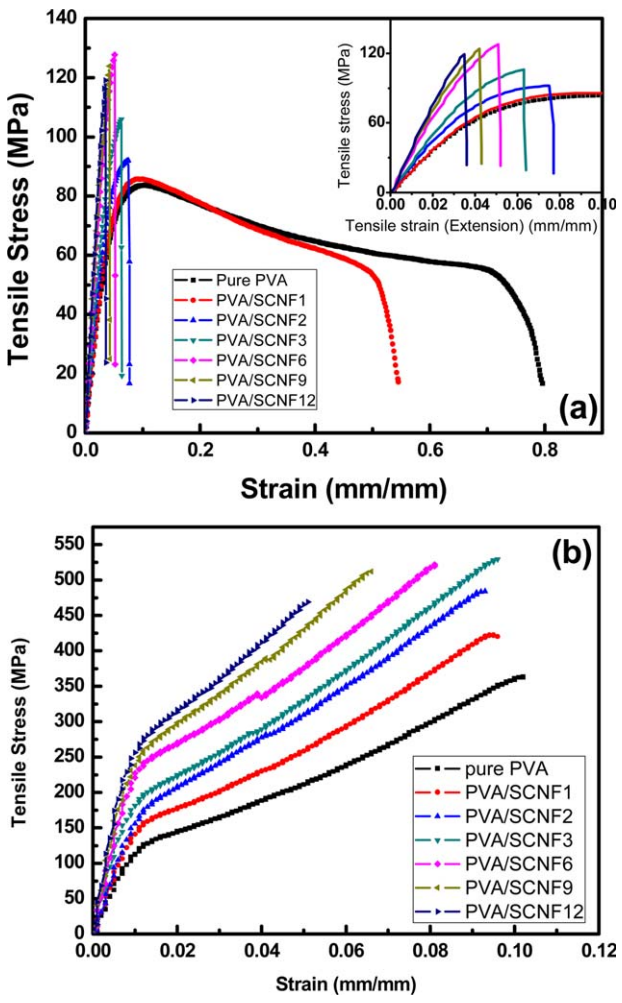

Figure 3. Stress–strain curves of pure PVA and PVA/SCNF nanocomposite films: (a) draw ratio of 1.0 and (b) draw ratio of 7.5. [Color figure can be viewed in the online issue, which is available at wileyonlinelibrary.com.]

Table III. Tensile Properties of Neat PVA and PVA/SCNF Composite Films with a Draw Ratio of 1.0 (Unstretched) and a Draw Ratio of 7.5

	Samples	Ultimate strength (MPa)	Young's modulus (GPa)	Strain at break (mm/mm)
Draw Ratio of 1.0	Pure PVA	83.7 ± 3.35	1.7 ± 0.15	0.713 ± 0.128
	PVA/SCNF1	85.7 ± 3.43	1.7 ± 0.19	0.502 ± 0.100
	PVA/SCNF2	92.0 ± 3.68	2.0 ± 0.18	0.077 ± 0.006
	PVA/SCNF3	105.9 ± 4.24	2.3 ± 0.21	0.064 ± 0.008
	PVA/SCNF6	127.8 ± 5.11	3.0 ± 0.27	0.052 ± 0.004
	PVA/SCNF9	123.9 ± 4.96	3.3 ± 0.29	0.043 ± 0.004
	PVA/SCNF12	119.1 ± 4.76	3.6 ± 0.32	0.036 ± 0.003
Draw Ratio of 7.5	Pure PVA	363.5 ± 19.2	11.3 ± 1.2	0.101 ± 0.008
	PVA/SCNF1	422.2 ± 24.3	14.1 ± 2.6	0.096 ± 0.010
	PVA/SCNF2	484.0 ± 25.2	15.6 ± 2.4	0.093 ± 0.007
	PVA/SCNF3	529.5 ± 29.5	18.2 ± 1.8	0.096 ± 0.120
	PVA/SCNF6	522.0 ± 26.1	22.1 ± 2.6	0.081 ± 0.006
	PVA/SCNF9	512.2 ± 25.9	23.8 ± 2.5	0.066 ± 0.007
	PVA/SCNF12	469.2 ± 23.5	25.6 ± 2.0	0.051 ± 0.004

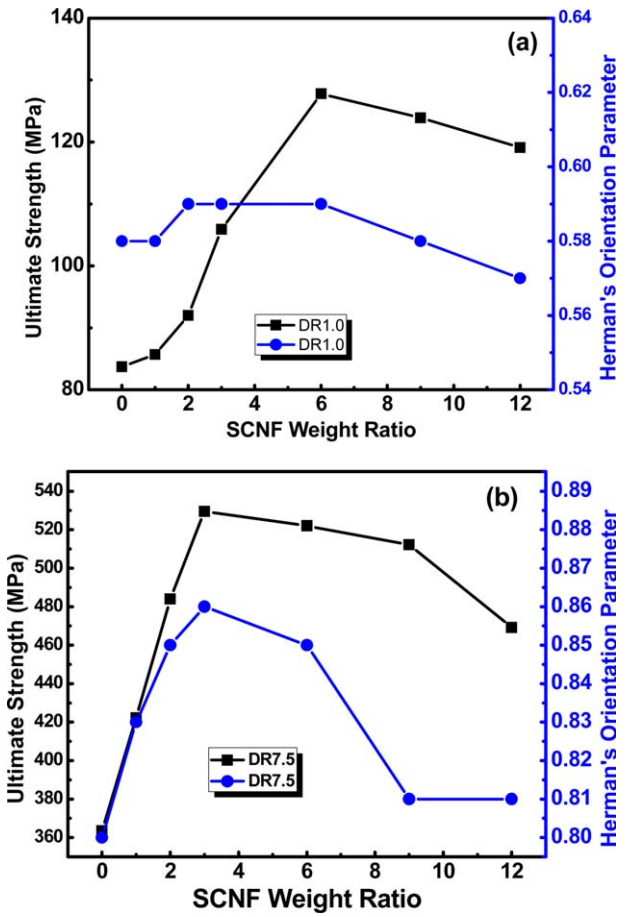

Figure 4. Comparisons of SCNF weight ratios and crystal orientation effects on ultimate fiber strength: (a) draw ratio of 1.0 and (b) draw ratio of 7.5. [Color figure can be viewed in the online issue, which is available at wileyonlinelibrary.com.]

the SCNF fillers. Figure 4 shows the ultimate tensile strengths of PVA/SCNF films with respect to both SCNF weight ratios and crystal orientations. Undrawn composite films with various SCNF filler weight ratios had a similar orientation parameter of about 0.58. Consequently, the strength increase was mainly a result of SCNF reinforcement. At a draw ratio of 7.5, the ultimate strength peaked at an SCNF weight ratio of about 3%. Below the percolation threshold (likely 2.5–4.9% SCNF), the strength increased with the addition of SCNF, as did the crystal orientation of the PVA matrix. Despite reductions in PVA orientation at higher loading levels, gains in strength were largely maintained due to increased reinforcement from the additional amount of SCNF [Table III and Figure 4(b)]. With consideration of both SCNF reinforcement and PVA alignment effects, the ultimate strength and modulus of PVA/SCNF3 were nearly 46 and 61% higher than that of neat PVA. Thus, to achieve the highest tensile strength, crystal orientation, SCNF weight ratios and their relationship need to be considered.

Based on our group's previous work, the ultimate strength and modulus of PVA/SCNF gel spun fiber with a SCNF weight ratio of 6% were nearly 60 and 220% higher than that of neat PVA.[22] Shifts in the Raman peak at ~1095/cm, which was associated with the C—O—C glycosidic bond of SCNF, indicated good stress transfer between the SCNF and the PVA matrix likely due to interfacial hydrogen bonding.[22] The tensile improvements of the films were lower than their fibrous counterparts because of the smaller amount of PVA crystallinity due to the different processing methods used. As mentioned previously, Uddin *et al.*[20] produced gel spun fibers from aqueous PVA solutions with up to 30% CNC prepared by acid hydrolysis. Adding 5% CNC increased the ultimate tensile strength by 20% compared to neat PVA fibers. However, the tensile strength was reduced at concentrations above 5% at least partly due to reduced PVA molecular orientation. Because of the likely hydrogen bonding

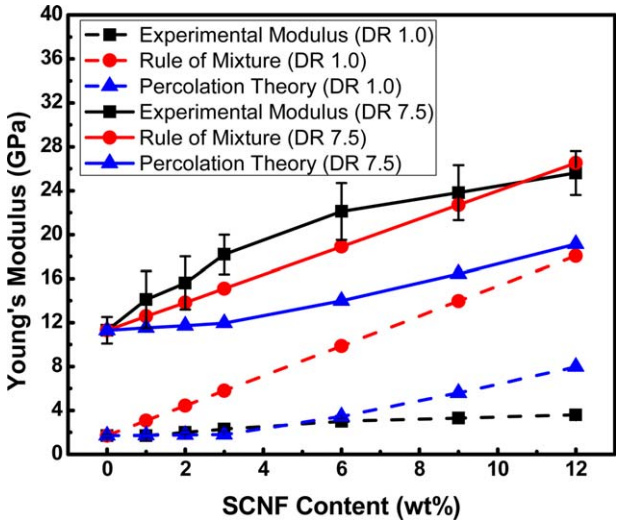

Figure 5. Comparison of experimental data to models: PVA/SCNF composite film with a draw ratio of (a) 1.0 and (b) 7.5. [Color figure can be viewed in the online issue, which is available at wileyonlinelibrary.com.]

between the SCNF and PVA matrix, PVA/SCNF films achieved improved ultimate strength and modulus simultaneously.

Young's moduli, which were determined experimentally, were compared with theoretical predictions based on the classic Rule of Mixtures [eq. (4)], and the Percolation approach [eq. (5)].[36,37]

$$E = E_r X_r + E_m X_m \tag{4}$$

$$E = \frac{(1-2\psi+X_r)E_m E_r + (1-X_r)\psi E_r^2}{(1-X_r)E_r + (X_r-\psi)E_m} \tag{5}$$

Parameter E is the predicted nanocomposite modulus, E_r is the SCNF modulus of 138 GPa,[7] E_m is the PVA matrix film modulus, and X is the volume fraction. In the calculation, E_m of neat PVA film with draw ratio of 1.0 and 7.5 are 1.7 and 11.3 GPa, respectively (Table III). The percolation volume fraction, ψ, is given by

$$\psi = \left(\frac{X_r - X_c}{1 - X_c}\right)^b \tag{6}$$

where X_c is the percolation threshold, and b is the critical percolation exponent of 0.4 for a three-dimensional system.[35]

As shown in Figure 5, theoretical modeling based on the Percolation approach was in good agreement with the experimental data for undrawn PVA/SCNF films, especially at low SCNF weight ratios. Deviations at higher SCNF content may have resulted from overestimation of the value for SCNF modulus, which varies widely in the literature and was not measured directly. The rule of mixtures assumes continuous, unidirectional reinforcement, and strong adhesion between filler and matrix[37,38] and represents an upper bound for our composites. Given that the undrawn films contain partially oriented, discontinuous fibers, it is not surprising that our experimental values are significantly lower than those predicted. For drawn films, the rule of mixtures predicted the modulus surprisingly well, except at intermediate SCNF contents, where the experimental

Table IV. Thermal Properties of Pure PVA and PVA/SCNF Films

	Differential scanning calorimetry (DSC)									Thermogravimetric analysis (TGA)	
	Pure and filled PVA films after heat treatment (DR 1.0)[a]				Pure and filled hot drawn PVA films (DR 7.5)[b]						
Compound	T_m in C ±1.0°C	ΔH_m (J/g)	Crystallinity (%)	Crystal size for (101/10-1) (nm)	T_m in C ±1.0°C	ΔH_m (J/g)	Crystallinity (%)	Crystal size for (101/10-1) (nm)	T_{onset} in C ±2.0°C	T_d in C ±2.0°C	Residual wt % ± 1%
Pure PVA	227.9	61.6	39.0	39.83	230.3	74.2	46.9	52.01	247.3	270.7	6.0
PVA-SCNF1	226.8	66.2	42.3	36.91	229.7	73.7	47.1	50.4	246.1	271.8	6.0
PVA-SCNF2	226.3	65.6	42.4	35.92	229.7	72.6	46.9	49.5	246.0	272.7	6.3
PVA-SCNF3	226.1	64.1	41.8	35.60	228.2	72.3	47.1	46.6	245.6	275.3	6.2
PVA-SCNF6	223.1	62.2	41.9	35.15	227.3	70.8	47.7	46.3	242.0	280.9	6.2
PVA-SCNF9	222.3	59.4	41.3	34.90	227.5	69.2	48.1	45.5	241.9	278.0	7.2
PVA-SCNF12	221.2	56.2	40.4	34.74	226.8	69.3	49.8	44.8	241.1	281.0	9.1
pure SCNF	N/A	N/A	N/A	N/A	N/A	N/A	N/A	N/A	198.3	338.3	28.4

[a] Heat treatment: 4 min at 200°C.
[b] Hot drawn at 200°C. χ_c: crystallinity. Crystal sizes are calculated based on X-ray diffraction pattern.

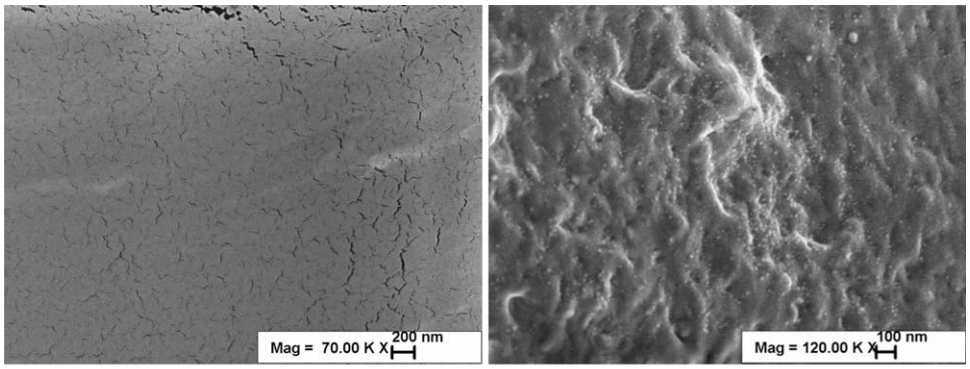

Figure 6. SEM images of cryogenic fracture surfaces of (a) pure PVA and (b) PVA/SCNF12 drawn films with a draw ratio of 7.5.

values exceeded those predicted. However, the rule of mixtures does not consider the reinforcement's effects on the matrix. In our case, the SCNF facilitated matrix orientation over the same range where the predicted values were exceeded (c.f. Table II and Figure 5). While the differences in Herman's orientation parameters were not large, mechanical properties are very sensitive to orientation in highly aligned polymers and composites.[39]

Thermal Properties

The thermal behavior was investigated by DSC to understand the impacts of SCNF on composite films with drawing ratios of 1.0 and 7.5. Since the entire drawing process took about 4 min to complete, undrawn PVA/SCNF composite films were first heat treated for 4 min at 200°C before scanning in the DSC so that both the drawn and undrawn had similar heat histories. Table IV shows the melting temperature (T_m), heat of fusion (ΔH_f), and crystallinity (χ_c) as determined by DSC. The melting temperatures of PVA composite films at both draw ratios decreased with increasing SCNF weight ratios suggesting a smaller or less perfect PVA crystal structure when SCNF was added.[40] PVA crystal size was determined using the Scherrer equation[41] and the (101) planes, which are summarized in Table

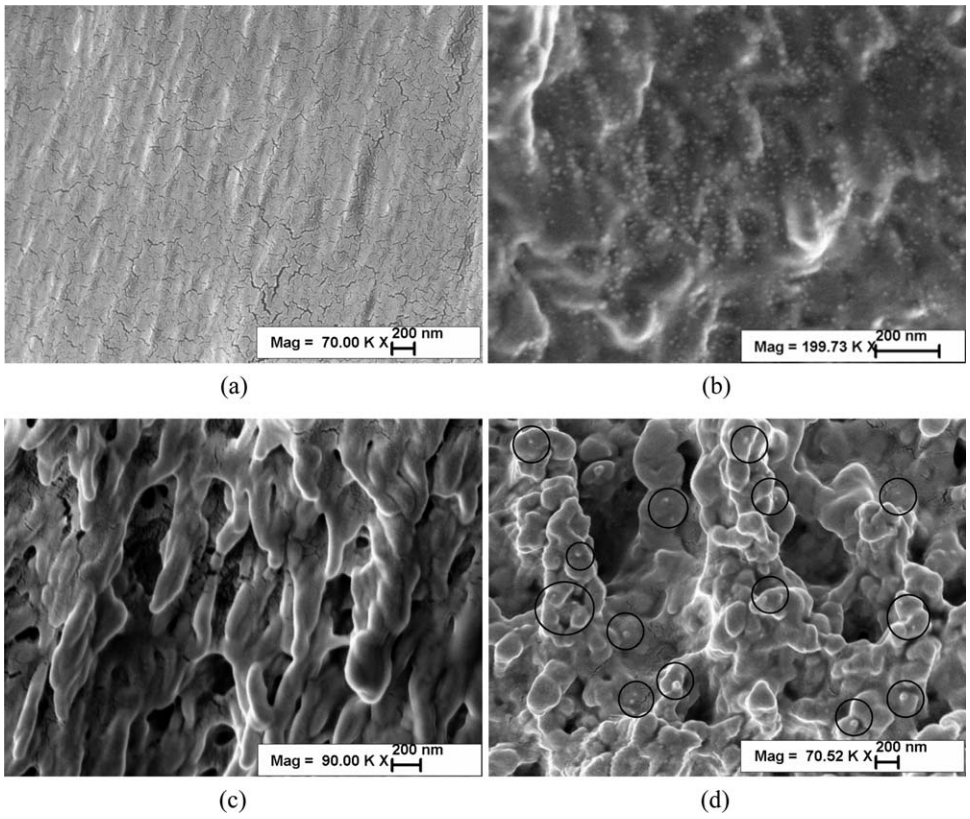

Figure 7. SEM images of the tensile fracture surfaces of (a) neat PVA and (b) PVA/SCNF12 films with a draw ratio of 1.0 (no stretching); (c) neat PVA and (d) PVA/SCNF12 films with a draw ratio of 7.5. The black circles highlight the SCNF located on PVA broken fibrils.

IV. The values for crystal size are reduced with addition of SCNF, which correlates well with the shift in the PVA melting point.

The crystallinity of PVA varies with draw ratio and SCNF weight ratio. Undrawn PVA composite films with 1 or 2% SCNF have a crystallinity of about 42.4%, slightly higher than that (39.0%) of the neat PVA. Further addition of SCNF decreased the crystallinity. Although the SCNF served as a mild nucleating agent for all PVA/SCNF composite films, increased SCNF content hindered crystallinity in undrawn films. Note that the crystallinity of PVA composite films with a draw ratio of 7.5 is much higher than their undrawn counterparts, as chains align in the drawing direction, facilitating crystallization.

Thermogravimetric analysis (TGA) was used to investigate the effects of SCNF on the thermal stability of the films. T_{onset} is the decomposition temperature at a 5 wt % weight loss, while T_d is the temperature of the maximum weight loss rate taken as the temperature corresponding to the peak of the derivative degradation endotherm. Given SCNF's relatively low T_{onset} of 198°C as measured by TGA, it is not surprising that the composites' T_{onset} values decreased with the addition of SCNF filler. However, the T_d of the composites shifted toward higher temperatures with increased amounts of SCNF. In addition, the residues at 800°C corresponded to the char yield from the PVA and SCNF.

Cryogenic and Tensile Fracture Morphologies

In order to examine SCNF dispersion in the PVA matrix, the cryogenic and tensile fracture surfaces of neat PVA and PVA/SCNF films were characterized by SEM. Figure 6 shows images of the cross sections of cryogenically fractured neat PVA and PVA/SCNF12 films with a draw ratio of 7.5. Figure 7 shows images of the tensile fracture morphologies and SCNF dispersions of filled PVA films at various draw ratios.

The uniformly dispersed spots in Figure 6(b) are likely SCNF given that their diameters are similar to those of SCNF (Figure 1) and that they are not present in the neat PVA image in Figure 6(a). Similar features are found in the tensile fracture images in Figure 7 as well. Overall, the SCNF appear well-dispersed and the absence of any fiber pullout suggests good SCNF–PVA adhesion.

The drawn films [Figures 7(c) and (d)] showed a more fibrillar structure—regardless of whether SCNF was added—undoubtedly as a result of greater molecular alignment. This fracture morphology appears similar to that described by Elices and Llorca[42] for PVA fibers, in which the fracture was initiated by transverse cracking in the skin layer, followed by single fibril separation.

CONCLUSIONS

Discrete, highly crystalline SCNF were prepared from enzymatically pretreated cellulose via mechanical isolation. Hot drawn and undrawn PVA/SCNF composite films were produced using SCNF as a reinforcement. SCNF was effective in improving the tensile performance of the PVA matrix but depended on the SCNF weight ratio, PVA crystal orientation, and hot draw ratio. Hot drawing increased PVA crystal orientation along the film axis direction. Adding small amounts (less than 3%) increased the orientation of the crystalline PVA fraction at high draw ratios. However, further addition of SCNF began to reduce the orientation, probably as a result of SCNF network formation, which limited molecular alignment. Improvements in tensile strength appeared to be due to a combination of increased orientation (at low SCNF weight ratios) and SCNF reinforcement. Further increases in tensile strength at SCNF levels more than 9% were prevented by reductions in orientation. However, the modulus increased with additional SCNF content which is less than 3% and the values maintained constant over 3%. Drawn PVA/SCNF films with additional SCNF possessed increased crystallinity, which was a combination of thermal-induced crystallinity and stress-induced crystallinity. Drawn PVA/SCNF films with a draw ratio of 7.5 possessed comparable Young's moduli of drawn composite film were predicted surprisingly well by the rule of mixtures except at intermediate levels of SCNF where the increased orientation of the matrix was not considered in the model. Examination of cryogenically fractured specimens and fracture surfaces from tensile testing of the composite films indicated that SCNF had a uniform dispersion in the PVA matrix, which is critical to enhancing mechanical performance.

Ultimately, effective use of nanocellulose in polymers will require an understanding of how preparation methods and resulting morphologies and functionalities of nanocelluloses affect their ability to be processed with polymers as well as the end performance and the economics of the resulting composites. Our SCNF had similar aspect ratios but different chemical functionalities than wood-derived CNCs prepared by sulfuric acid hydrolysis. The SCNF could be added to PVA at higher levels than was reportedly possible with more conventional CNF prepared by TEMPO-mediated oxidation.[21] An optimal level was found for the simultaneous improvement of tensile strength and modulus in oriented composites, where significant reinforcement was achieved and facilitation of orientation was maximized. However, less energy intensive preparation of SCNF (e.g., with more optimized enzymatic pretreatment) would improve economic feasibility and is an ongoing area of research.

ACKNOWLEDGMENTS

This project was supported by the USDA National Institute of Food and Agriculture Award (No. 2011–67009-20056). The authors would like to acknowledge Yan Qing and J. Y. Zhu for processing the short cellulose nanofibrils. Debby Sherman at Purdue University is kindly acknowledged for TEM imaging. The first author also wishes to acknowledge the National Nature Science Foundation of China (Nos. 51073601, 21174044), the Fundamental Research Funds for the Central Universities (No. 2011ZZ0011), the China Postdoctoral Science Foundation (2012M511791), and the 973 Program (2012CB025902) for their financial support.

REFERENCES

1. Moon, R. J.; Martini, A.; Nairn, J.; Simonsen, J.; Youngblood, J. *Chem. Soc. Rev.* **2011**, *40*, 3941.

2. Iwamoto, S.; Nakagaito, A. N.; Yano, H. *Appl. Phys. A* **2007**, *89*, 461.
3. Zimmermann, T.; Bordeanu, N.; Strub, E. *Carbohydr. Polym.* **2010**, *79*, 1086.
4. Dufresne, A.; Cavaille, J. Y.; Vignon, M. R. *J. Appl. Polym. Sci.* **1997**, *64*, 1185.
5. Johnson, R. K.; Zink-Sharp, A.; Renneckar, S. H.; Glasser, W. G. *Cellulose* **2009**, *16*, 227.
6. Josefsson, G.; Tanem, B. S.; Li, Y.; Vullum, P. E.; Gamstedt, E. K. *Cellulose* **2013**, *20*, 761.
7. Nishino, T.; Takano, K.; Nakamae, K. *J. Polym. Sci. Polym. Phys.* **1995**, *33*, 1647.
8. Uddin, A. J.; Narusawa, T.; Gotoh, Y. *Polym. Eng. Sci.* **2011**, *51*, 647.
9. Vinyl Acetate Monomer (VAM) Market Analysis by Application (Polyvinyl Acetate, Polyvinyl Alcohol, Ethylene Vinyl Acetate, Ethylene Vinyl Alcohol) and Segment Forecasts to 2020; **2015**. Available at: http://www.grandviewresearch.com/industry-analysis/vinyl-acetate-monomer-vam-market.
10. Jorfi, M.; Roberts, M. N.; Foster, E. F.; Weder, C. *ACS Appl. Mater. Interfaces* **2013**, *5*, 1517.
11. Zheng, Q.; Cai, Z.; Gong, S. *J. Mater. Chem. A* **2014**, *2*, 3110.
12. Paralikar, S. A.; Simonsen, J.; Lombardi, J. *J. Membr. Sci.* **2008**, *320*, 248.
13. Leitner, J.; Hinterstoisser, B.; Wastyn, M.; Keckes, J.; Gindl, W. *Cellulose* **2007**, *14*, 419.
14. Bruce, D; Hobson, R; Farrent, J; Hepworth, D. *Compos. Part A: Appl. Sci. Manufact.* **2005**, *36*, 1486.
15. Wang, B; Sain, M. *Compos. Sci. Technol.* **2007**, *67*, 2521.
16. Zimmermann, T.; Pohler, E.; Geiger, T. *Adv. Eng. Mater.* **2004**, *6*, 754.
17. Bhatnagar, A. *J. Reinforced Plast. Compos.* **2005**, *24*, 1259.
18. Lu, J.; Wang, T.; Drzal, L. *Compos. Part A: Appl. Sci. Manufact.* **2008**, *39*, 738.
19. Roohani, M; Habibi, Y; Belgacem, N; Ebrahim, G; Karimi, A; Dufresne, A. *Eur. Polym. J.* **2008**, *44*, 2489.
20. Uddin, A. J.; Araki, J.; Gotoh, Y. *Compos. Part A: Appl. Sci. Manufact.* **2011**, *42*, 741.
21. Uddin, A. J.; Araki, J.; Gotoh, Y. *Biomacromolecules* **2011**, *12*, 617.
22. Endo, R.; Saito, T.; Isogai, A. *Polymer* **2013**, *54*, 935.
23. Peng, J.; Ellingham, T.; Sabo, R.; Turng, L. S.; Clemons, C. M. *Cellulose* **2014**, *21*, 4287.
24. Zheng, Z. H.; Feldman, D. *Prog. Polym. Sci.* **1995**, *20*, 185.
25. Sun, W.; Chen, H. S.; Luo, X.; Qian, H. P. *Cem. Concrete Res.* **2001**, *31*, 595.
26. Peresin, M. S.; Habibi, Y.; Zoppe, J. O.; Pawlak, J. J.; Rojas, O. J. *Biomacromolecules* **2010**, *11*, 674.
27. Qing, Y.; Sabo, R.; Zhu, J. Y.; Agarwal, U.; Cai, Z.; Wu, Y. A. *Carbohydr. Polym.* **2013**, *97*, 226.
28. Zhu, J. Y.; Sabo, R.; Luo, X. *Green Chem.* **2011**, *13*, 1339.
29. Ke, B. Newer Methods of Polymer Characterization; Interscience Publishers: New York, **1964**.
30. ASTM. Standard Test Method for Tensile Strength and Young's Modulus for High-Modulus Single-Filament Materials; **1989**, p. 5.
31. Schildknecht, C. E. Polyvinyl Alcohol, Properties and Applications; Wiley: New York, **1973**.
32. Shinoda, R.; Saito, T.; Okita, Y.; Isogai, A. *Biomacromolecules* **2012**, *13*, 842.
33. Uddin, A.; Araki, J.; Gotoh, Y. *Biomacromolecules* **2011**, *12*, 617.
34. Uddin, A. J.; Ohkoshi, Y.; Gotoh, Y.; Nagura, M.; Endo, R.; Hara, T. *Int. Polym. Proc.* **2006**, *21*, 263.
35. Siqueira, G.; Bras, J.; Dufresne, A. *Polymers* **2010**, *2*, 728.
36. Davies, W. E. A. *J. Phys. D: Appl. Phys.* **1971a**, *4*, 6.
37. Bulota, M.; Jaaskelainen, A. S.; Paltakari, J.; Hughes, M. *J. Mater. Sci.* **2011**, *46*, 3387.
38. Sharma, S. Economics of Composites and Reinforcements; Composite Materials, 1 Ed; Narosa Publishing House: New Delhi, **2002**.
39. Mahanandia, P.; Schneider, J. J.; Khaneft, M.; Stuhn, B.; Peixoto, T. P.; Drossel, B. *Phys. Chem. Chem. Phys.* **2010**, *12*, 4407.
40. Ehrenstein, G.; Riedel, G.; Trawiel, P. Thermal Analysis of Plastics; Hanser Publishers: Cincinnati, **2004**.
41. Scherrer, P. *Nachr Ges Wiss Göttingen* **1918**, *26*, 98.
42. Elices, M.; Llorca, J. Fiber Fracture; Elsevier Science Ltd.: Kidlington, UK, **2002**.